Journal of Physics: Conference Series

PAPER • **OPEN ACCESS**

High frequency vortex dynamics in $YBa_2Cu_3O_{7-x}$ with Ba_2YTaO_6-Ba_2YNbO_6 nanodefects

To cite this article: K. Torokhtii *et al* 2020 *J. Phys.: Conf. Ser.* **1559** 012043

Journal of Physics: Conference Series **1559** (2020) 012043 doi:10.1088/1742-6596/1559/1/012043

High frequency vortex dynamics in $YBa_2Cu_3O_{7-x}$ with Ba_2YTaO_6-Ba_2YNbO_6 nanodefects

K. Torokhtii[1], A. Alimenti[1], F. Rizzo[2], A. Augieri[2], G. Celentano[2], A. Frolova[1,3], E. Silva[1], N. Pompeo[1]

[1]Department of Engineering, Roma Tre University, Via Vito Volterra 62, Roma 00146, Italy
[2]ENEA Frascati Research Center, Via Enrico Fermi 45, 00044, Frascati, Italy

E-mail: * kostiantyn.torokhtii@uniroma3.it

Abstract. We studied pinning characteristics of $YBa_2Cu_3O_{7-x}$ (YBCO) with 5 mol.% Ba_2YTaO_6/Ba_2YNbO_6 (BYNTO). In contrast to widely used d.c methods, at microwaves very short oscillations of the fluxons are involved giving the information on both the pinning strength, through the pinning constant and on dissipation, related to the vortex core physics, through the viscosity η. We estimate the pinning constant k_p,the vortex viscosity η and also the maximum creep factor χ_{max}. The results were compared not only with the pristine YBCO sample but also with the effect of another type of columnar defects (BZO) in YBCO. All film samples were grown by Pulsed Laser Deposition (PLD) technique at nearly the same conditions to ensure the uniform. We detect an improvement of all pinning characteristics of YBCO-BYNTO sample in the temperature range 62 - 90 K and for field up to 0.75 T. While the average diameter of the defects is similar for YBCO-BYNTO and YBCO-BZO the key of the superior characteristics in YBCO-BYNTO could be both the concentration of columns and an addition of another phase of point-like defects.

1. Introduction

Growing demand in superconductors capable to operate at high temperatures forces the development of the new techniques of the deposition and material improvement. Superconductors are requested in various fields from electronics to large scale applications [1].

One of the most promising materials is $YBa_2Cu_3O_{7-x}$ (YBCO) with critical temperature T_c around 90 K. It becomes a great candidate for areas where high critical current J_c is required [2]. Various deposition techniques were developed for different applications, coated conductors [3] and chemically deposited YBCO [4] became a front line of the research. Since the superconductive performances of these materials strongly depend on the growing conditions and composition, only a detailed control of the quality of the samples could guarantee long-term characteristics.

Addition of artificial pinning centers (APCs) in matrix of the YBCO has become a preferable way to improve critical current J_c performance [5, 6]. One of the best techniques to improve pinning in YBCO is an introduction of $BaZrO_3$ (BZO), which creates columnar APCs (or 1D defects) [5, 7]. The success of 1D defects as pinning centers encourages the research of new materials capable to form 1D APCs. One of the most advantageous is an addition of the second

[3] Present address: National Research Nuclear University MEPhI, Kashirskoe shosse 31, Moscow, 115409, Russia

phase of Ba_2YTaO_6/Ba_2YNbO_6 (BYNTO) [8, 9], which form two types of APCs 1D and 3D (point-like defects).

While traditionally the d.c. characterization of the superconducting samples is used, complementary information could be obtained at microwave frequencies [10]. At microwaves, the effectiveness of the single pinning site could be probed by the small oscillation of the fluxon at the bottom of the pinning well [11]. In this article, we performed a study of the pinning properties at microwaves using dielectric resonator technique at 47 GHz. This paper extends data in reference [12] to the wide range of temperatures, extracting pinning constant, vortex viscosity term and an estimation of the maximum creep.

2. Samples preparation

We choose the Pulsed Laser Deposition (PLD) technique for all samples analyzed in this article to ensure uniform sample quality and the best control of the growing process. For YBCO-BYNTO preparation, the target was ablated by 308 nm Lambda Physik 110i cc XeCl laser at a repetition rate of 10 Hz and laser energy density 2.5 J/cm^2. The deposition process was at a partial pressure of oxygen equal to 300 mTorr and temperature 840 ^{o}C [13]. The film of YBCO-BYNTO with thickness t_s =150 nm was grown on STO substrate. Detailed TEM analysis was made on the samples of this series [9]. Self-assembled elongated c-axis oriented BYNTO columnar defects were observed without signs of any discontinuity in the BYNTO columns (contrary to BYTO short nanocolumns [9]). The films samples are characterized by the presence of two types of defects within the YBCO matrix: with BYNTO nanocolumns, also Y_2O_3 point-like defects are present near the nanocolumns [9].

As a comparison to the YBCO-BYNTO sample, we take pristine YBCO and YBCO-BZO samples grown on STO substrate. These samples were also prepared by PLD technique based on the sintered YBCO and YBCO with 5 mol.% BZO targets. For the laser ablation, the same laser with the same regime was used as for YBCO-BYNTO. The deposition was performed at a partial pressure of oxygen equal to 300 mTorr and temperature 850 ^{o}C. More details could be found in references [14]. The films were 120-nm thick for YBCO and 130-nm thick for YBCO-BZO measured by stylus profilometer. Both YBCO and YBCO-BZO films have good structural properties and smooth surface, confirmed by X-ray diffraction and SEM analysis. TEM analysis shows self-assembled BZO nanorods in the YBCO matrix oriented perpendicular to the a-b-planes. More details about the microscopic study of of the series of the similar samples are reported in [15].

Comparable deposition process, regimes, and sample quality allow the most reliable analysis of the pinning effectiveness of 1D defects. Previous studies on similar samples show that even the size of both BZO and BYNTO defects is similar (around 5 nm in diameter). All films under study have the critical temperature near 90 K: 90.4 K for pristine YBCO, 90.6 K and 89.4 K for YBCO-BZO and YBCO-BYNTO correspondingly. One of the main difference is the density of the nanocolumns, which is around 600 μm^{-2} for BZO and 2500 μm^{-2} for BYNTO [9]. Moreover, while BZO forms only one type of defects, BYNTO has both BYNTO nanocolumns and Y_2O_3 nanoparticles.

3. Surface impedance measurement

Traditionally used J_c measurements, where the large Lorentz force generates large vortex displacements, allow to extract information about maximum depinning force. Instead, here we concentrate on the microwave measurements, where small-scale (not exceeding 1 nm) oscillations of fluxons around an equilibrium position are produced. This becomes a way to look inside the physics of the pinning and add a complementary information to d.c. measurements.

At microwaves, small displacements confine the vortex in the energy well. One could easily describe vortex motion starting from a general balance of the forces acting on the single vortex.

Here, the Lorentz force and the force, responsible for the thermally activated movement are compensated by a drag force, hall force (usually negligible) and pinning force.

For this study of the vortex motion, we used a dielectric resonator (DR) operating at 47.7 GHz. This cylindrical resonator of Hakki-Coleman type has been specifically designed for the measurements of thin-film samples [16]. The DR consists in a cylindrical brass cavity with a coaxially positioned sapphire puck (0.8 mm diameter and 2 mm height). We used the so-called surface perturbation method where a part of the metallic surface of the resonator is replaced by the sample. To exclude the effect of the borders of the 7x7 mm^2 square sample on the response of the resonator we use a metallic mask with a 6-mm diameter hole. The whole resonant line was designed to operate in liquid nitrogen bath cryostat in the temperature range from 60 K to the room temperature [17]. Magnetic field perpendicular to the sample surface up to 0.75 T was generated by a conventional electromagnet.

The measured quantity defined by the electrodynamic response of superconductors is the surface impedance, defined as the ratio between the electric and magnetic fields parallel to the surface of the sample $Z_s = E_{||}/H_{||}$. In DR measurements of Z_s, the quantities of interest are the quality factor Q and the resonant frequency f_0 corresponding to electromagnetic mode at which DR operates. The results here presented are based on the field variations of the resonator characteristics. In particular, from the variation of Q and f_0 in the magnetic field H the field dependence of Z_s of the superconductor can be easily obtained as follows:

$$\Delta Z(H) = G\left(\Delta\frac{1}{Q}(H) - \mathrm{i}\frac{2\Delta f_0(H)}{f_{0,H=0}}\right) + background \tag{1}$$

where G is a constant geometrical factor estimated by electromagnetic simulations; Δ indicates the variation of a parameter to zero-field value. The *background* contribution represents the contribution of DR without sample and can be neglected due to the absence of any detectable magnetic background in the empty resonator, having had care in using nonmagnetic materials

The fact that samples under study have thickness t_s below 150 nm allows us to apply thin-film approximation and connect the complex resistivity of superconductor ρ_s to Z_s by a simple relation $Z_s = \rho_s/t_s$ [18]. We are interested here in the magnetic field dependence of ρ_s where the main contribution is due to the motion of vortices, since field pair breaking, far from H_{c2} and T_c, can be neglected. Thus one could write $\Delta\rho_s(H) \approx \Delta\rho_{vm}(H)$, where ρ_{vm} is the vortex motion resistivity.

The DR operates in the TE_{011} mode, due to its advantage to generate planar circular currents on the sample surface, its high Q allowing good sensitivity, and spatial concentration of the electromagnetic field near the dielectric, which allows to avoid border effects. This way the results of the measurements with in-plane microwave current (induced by TE_{011} mode) and perpendicular magnetic field becomes more easily interpreted with analytical models.

4. Pinning characteristics determination

The vortex motion resistivity ρ_{vm} can be interpreted based on the models developed in [11] and refs. there in. A general form of ρ_{vm} is represented as follows:

$$\rho_{vm} = \frac{\Phi_0\mu_0 H}{\eta}\frac{\chi + \mathrm{i}f/f_c}{1 + \mathrm{i}f/f_c} \tag{2}$$

where η is the viscous drag coefficient (vortex viscosity); f is the operating frequency; f_c is the characteristic vortex frequency; χ is the creep factor, which is determined by the height of the pinning well.

In ref. [11] the method of the extraction of the pinning parameters from ρ_{vm} was developed. Based on the experimental, one first calculate the so-called r-parameter $r = Im(\rho_{vm})/Re(\rho_{vm})$

from which the pinning constant k_p, , the viscosity η and the upper limit for the creep factor follow.

It should be noted that it is impossible to determine parameters from experimental data only, but one could estimate its limiting values. We now estimate first k_p, which is the measure of the pinning well steepness. The r-parameter gives an approximation for the so called depinning frequency, $r \simeq f_p/f$, where f_p is the crossover frequency from low - f, non dissipative and pinning dominated vortex motion to high - f, dissipative vortex motion dominated by flux-flow. Once f_p is obtained, one derives k_p and η from Eq. 2. In view of the approximation used, the so-obtained values bear some uncertainty whose extent can be estimated following ref. [11]. Finally, Eq. 2 allows to estimate the maximum creep χ_{max} which be represented as a function of r-parameter only:

$$\chi_{max} = 1 + 2r^2 - 2r\sqrt{1+r^2} \tag{3}$$

5. Results and discussion

In Fig. 1 the pinning constant as a function of the perpendicular field H is shown. We limit the presentation of the data to the field range starting from 0.1 T due to the loss of the sensitivity when $\mathrm{Im}(Z_s)$ is near to zero. To compare data for all three samples here we present measurements at the selected temperatures at the same reduced temperature $t = T/T_c$.

We observe in the temperature range down to 62 K a decreasing field dependence of k_p for the pristine YBCO sample. It is an evident characteristic of the YBCO samples without APC, as it was previously observed in various samples prepared with different growing techniques [19]. $k_p(H)$ for both YBCO-BZO and YBCO-BYNTO behaves differently from pristine YBCO sample. In YBCO-BZO a slight increase of k_p at low fields is followed by a decrease at high fields above 0.6 T. YBCO-BYNTO is characterized by the continuous growth of k_p up to the maximum field 0.75 T. It was observed that k_p in YBCO-BYNTO is at the same level of YBCO-BZO or higher. Thus in the presented temperature range better-pinning performance of YBCO-BYNTO is evident.

Fig. 2 shows the temperature evolution of k_p at field 0.75 T. It is confirmed by different studies [5, 20, 21], that nanocolumnar are most effective APCs. Here we show that BYNTO nanocolumns could be more effective than BZO in a wide temperature range. In the inset to Fig. 2 we show the benefit in the pinning parameter improvement by adding APCs. We show the relative difference of k_p with respect to the pristine YBCO sample for various ratios T/T_c. Previous J_c measurements show higher pinning force density for YBCO-BYNTO and superior performance up to 5 T [12]. The better pinning characteristics in terms of k_p and J_c results could be the result of the more than 3 times higher density of BYTO defects, while an average diameter of nanocolumns is similar for BZO and BYNTO. Besides, the decoration of BYNTO columns by Y_2O_3 nanoparticles gives additional pinning centers, improving k_p at high fields.

Since k_p characterizes the pinning potential steepness, column-like APCs indicates more steep (in average) pinning potential. Among all samples, YBCO-BYNTO shows better $k_p(H)$ and corresponding steeper pinning potential. While BZO nanocolumns become less effective at high fields even having a comparable level $k_p(H)$ derivative.

To understand better the microscopic nature of the defects we extracted also information about vortex core properties. From microwave measurements, one could estimate another important parameter, the vortex viscosity. The vortex viscosity gives an information about the quasiparticle density (n_{qp}) and scattering time in the vortex core (τ_{qp}) through the following relation $\eta \propto n_{qp}\tau_{qp}$ [22].

We show in Fig. 3 the vortex viscosity in the measured temperature range at 0.75 T. One notes a similar temperature dependence of η for all samples. The higher η for YBCO with APCs is evident,without significant variation between YBCO-BZO and YBCO-BYNTO was observed. An increase of η with the introduction of APCs is not new and was already observed in PLD

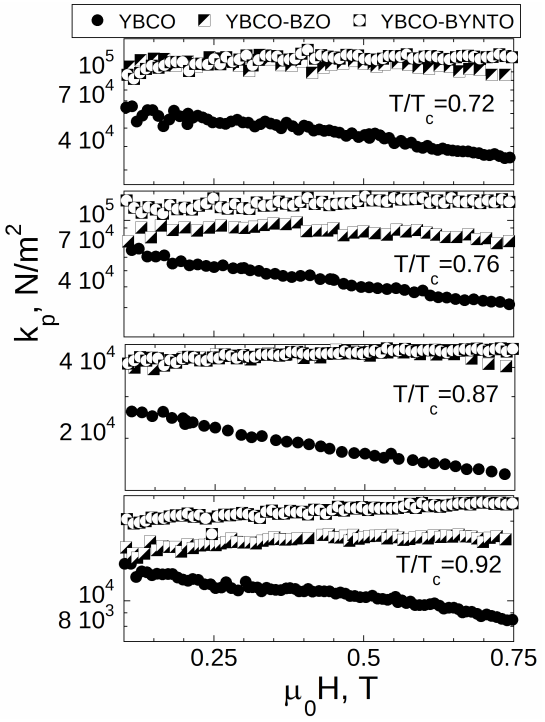

Figure 1. Pinning parameters data for YBCO, YBCO-BZO, YBCO-BYNTO samples as a function of perpendicular field. Selected sets of data with same T/T_c are shown only

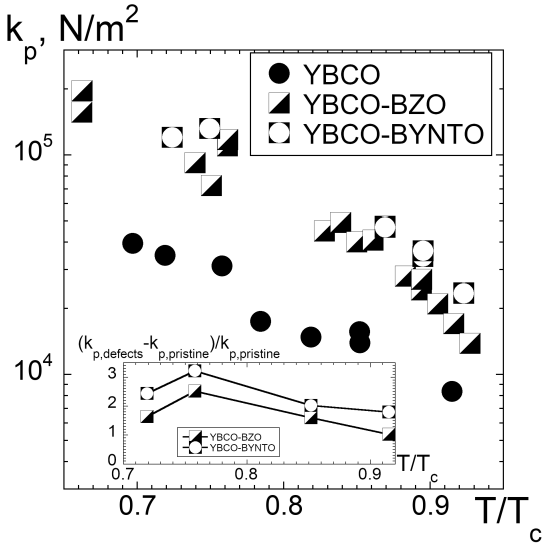

Figure 2. Pinning parameter for YBCO, YBCO-BZO and YBCO-BYNTO samples as a function of temperature at 0.75 T. Inset - variation of k_p with respect to pristine samples taking only experimental data with same ratio T/T_c

samples with BZO, where it was associated to the increase of the scattering time τ_{qp}, possibly, due to improved cristallinity of YBCO with APCs. [23, 19]

In the following, we compare the effect of BZO and BYNTO columnar APCs on the creep, in particular, the upper limit of the creep. As for k_p and η, also $\chi_{max}(r)$ can be obtained from the experimental r-parameter using Eq. 3.

In Fig.4a the field dependencies of maximum creep for various reduced temperatures are shown. It is evident that for YBCO-BYNTO the field dependence of $\chi_{max}(H)$ is the less pronounced and the absolute value is the lowest between all measured samples. With a decrease of the temperature χ_{max} in YBCO-BZO decreases much slower than for YBCO-BYNTO indicated BYNTO APCs as more efficient with respect to the creep at low temperature. The key to the different field dependencies of χ_{max} could be, also, the concentration of the defects. For YBCO-BZO an increasing number of fluxons occupy free pinning sites, both BZO nanocolumns at low field and YBCO matrix at high field. While in YBCO-BYNTO fluxons occupy mainly BYNTO pinning centers even at elevated fields.

We should note that both χ_{max} (see Eq. 3) and J_c measurements are connected to the pinning well height. Future studies will explore the possible (inverse) correlations between χ_{max} and J_c, in the effort toward a unified picture of pinning as probed by different dynamics.

6. Conclusions

We have presented an extended comparative study of the pinning properties of YBCO with two types of 1D APCs: BYNTO and BZO nanocolumns. The samples were prepared using the same

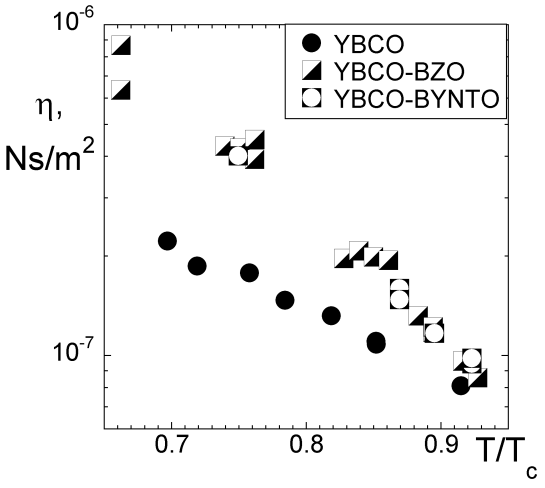

Figure 3. Vortex viscosity temperature dependence of YBCO, YBCO-BZO, YBCO-BYNTO samples as a function of temperature at 0.75 T applied perpendicularly to the sample surface.

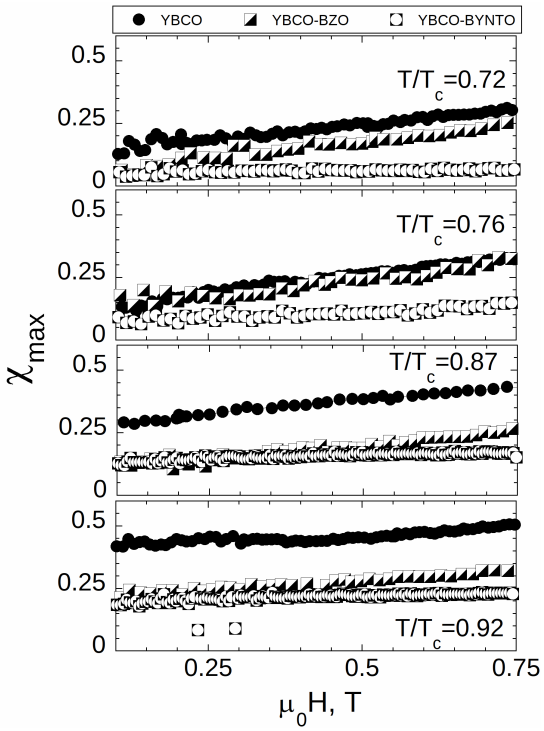

Figure 4. Maximum creep factor data for YBCO, YBCO-BZO, YBCO-BYNTO samples as a function of perpendicular field. Selected sets of data with same T/T_c are shown only.

deposition technique, the similar growing regimes and conditions. The field dependencies of k_p, η and χ_{max} were studied in the relatively low field range up to 0.75 T and at temperatures above 60 K. Comparing the results of k_p and η we show that BYNTO and BZO APCs are characterized by pinning wells with similar microscopic characteristics but different steepness in a wide temperature range. In YBCO-BYNTO sample we observe almost flat k_p and χ_{max} field dependencies pointing to vortices individually pinned by defects. Pinning in YBCO-BYNTO is more effective than in YBCO-BZO at high fields, possibly due to 4 times denser APCs and a combination of 1D and 3D defects.

Acknowledgment

This work has been carried out within the framework of the EUROfusion Consortium and has received funding from the Euratom research and training programme 2014-2018 and 2019-2020 under grant agreement No 633053. The views and opinions expressed herein do not necessarily reflect those of the European Commission.

References

[1] Maeda A, Kitano H, Inoue R 2005 *J. Phys. Condens. Matter* **17** R143–R185
[2] Muzzi L, De Marzi G, Di Zenobio A, della Corte A 2015 *Supercond. Sci. Technol.* **28** 053001
[3] Senatore C, Alessandrini M, Lucarelli A, Tediosi R, Uglietti D, Iwasa Y 2014 *Supercond. Sci. Technol.* **27** 103001
[4] Li Z *et al* 2019 *Sci. Rep.* **9** 5828
[5] MacManus-Driscoll J *et al* 2004 *Nat. Mater.* **3** 439–443

[6] Aye M, Khan M, Rivasto E, Tikkanen J, Huhtinen H, Paturi P 2019 *IEEE Trans. Appl. Supercond.* **29** 8000805.
[7] Frolova A *et al* 2016 *IEEE Trans. Appl. Supercond.* **26** 8001205
[8] Feldmann D, Holesinger T, Maiorov B, Foltyn S, Coulter J, Apodaca I 2010 *Supercond. Sci. Technol.* **23** 095004
[9] Rizzo F *et al* 2016 *APL Mater.* **4** 061101
[10] Pompeo N, Augieri A, Torokhtii K, Galluzzi V, Celentano G, Silva E 2013 *Appl. Phys. Lett.* **103** 022603
[11] Pompeo N, Silva E 2008 *Phys. Rev.* B **78** 094503
[12] Frolova A *et al* 2018 *IEEE Trans. Appl. Supercond.* **28** 7500805
[13] Rizzo F *et al* 2018 *Nanoscale* **10** 8187–8195
[14] A. Augieri *et al* 2008 *J. Phys.: Conf. Series* **97** 012209
[15] Augieri A *et al* 2010 *J. Appl. Phys.* **108** 063906.
[16] Torokhtii K *et al* 2016 *IEEE Trans. Appl. Supercond.* **26** 8001605.
[17] Pompeo N, Torokhtii K, Silva E 2014 *Meas. Sci. Rev.* **14** 164–170
[18] Pompeo N, Torokhtii K, Silva E 2017 *Proc.EEE International Instrumentation and Measurement Technology Conference (I2MTC)* Turin. DOI: 10.1109/I2MTC.2017.7969902
[19] Torokhtii K *et al* 2017 *IEEE Trans. Appl. Supercond.* **27** 8000405
[20] Wee S, Goyal A, Specht E, Cantoni C, Zuev Y, Selvamanickam V, Cook S 2010 *Phys. Rev.* B **81** 140503(R)
[21] Jha A, Matsumoto K, Horide T, Saini S, Mele P, Ichinose A, Yoshida Y, Awaji S 2016 *IEEE Trans. Appl. Supercond.***26** 8000404
[22] Golosovsky M, Tsindlekht M, Davidov D. 1996 *Supercond. Sci. Technol.***9** 182507
[23] Pompeo N, Rogai R, Silva E, Augieri A, Galluzzi V, Celentano G. 2007 *Appl. Phys. Lett.* **91** 182507